Supporting Information

Localized Nanoscale Heating Leads to Ultrafast Hydrogel Volume-Phase Transition

Jing Zhao,[†] Hanquan Su,[†] Gregory E. Vansuch,[†] Zheng Liu,[‡] Khalid Salaita,[†] R. Brian Dyer[*†]*

[†]Department of Chemistry, Emory University, Atlanta, Georgia, 30322, United States and [‡]Institute for Advanced Studies, Wuhan University, Wuhan, PR China.

Table of Contents

Table for references listed in Figure 1

Table S1. Reference Listed in Figure 1

Author	Polymer	Year	Ref #
Asher *et al*	poly(N- isopropylacrylamide) (pNIPAM)	2003	11
Tanaka *et al*	poly(N- isopropylacrylamide) (pNIPAM)	1998	13
Hu *et al*	poly(N- isopropylacrylamide) (pNIPAM)	2009	14
Liu *et al*	poly(2-vinylpyridine) (p2VP)	2008	15
Marquez *et al*	poly(N- isopropylacrylamide) (pNIPAM)	2006	16
Stokke *et al*	poly[N-(3-dimethylaminopropyl)acrylamide)-co-acrylamide] (p(DMAPAA-co-AAM))	2008	17

Principal Component Analysis (PCA) of Temperature-Dependent Steady-State FTIR Spectra

Temperature-dependent steady-state FTIR spectra of OMA nanoparticles in D_2O solution were collected on a Varian Excalibur FTIR instrument. The temperature dependence consists of two parts: the heating portion and the cooling portion, and each contains temperature-dependent spectra at 11 temperature points. To resolve the spectrum of swelled OMA (below LCST) and collapsed OMA (above LCST) at the amide I carbonyl stretching band region (1550 ~ 1700 cm^{-1}), the principal component analysis (PCA) was applied to the spectral data matrix [157 × 11], which involves singular value decomposition (SVD) and global-fitting analysis.

According to the SVD, the data matrix can be factorized into a multiplication of three matrices:

$$A = U \cdot S \cdot V^T$$

The $\boldsymbol{U}$ matrix [157 × 157] is referred as sepctral component matrix, each column of $\boldsymbol{U}$ matrix, $\boldsymbol{u_i}$ is a orthorgonal eigenvector that contains the basis spectral information.

The $\boldsymbol{S}$ matrix [157 × 11] is the singular value matrix, it is also a rectangle diagonal matrix. Each diagonal $\boldsymbol{s_i}$ can be understood as the weighting factor of each eigenvector in $\boldsymbol{U}$ and $\boldsymbol{V}$ matrices.

The $\boldsymbol{V}$ matrix [11 × 11] is the variable dependent matrix. In time-resolved spectra, it contains the kinetic information; in temperature-dependent spectra, it contains the information of temperature-dependent transformation; in pH-dependent spectra, it contains pH-dependent exchange information.

The essence of SVD is that only a few orthorgonal eigenvectors, $\boldsymbol{u_i}$, $\boldsymbol{v_i}$ and singular value $\boldsymbol{s_i}$ are required to reconstruct the data matrix. Because the first few eigenvectors (principal components) cover most of the meaningful change (variance) of the data matrix, it is usually feasible to reconstruct the spectral dataset with just these eigenvectors.

In our case, we picked the first two eigenvectors to reconstruct the spectral data matrix A_r.

$$A_r = U_r \cdot S_r \cdot V_r^T$$

$\boldsymbol{U_r}$ is [157 × 2], $\boldsymbol{S_r}$ is [2 × 2] and $\boldsymbol{V_r}$ is [2 × 11].

The truncated $\boldsymbol{V}$ matrix $\boldsymbol{V_r^T}$ can be factorized as the coefficient matrix $\boldsymbol{C}$ and functional change matrix $\boldsymbol{T}$.

Therefore, $$V_r^T = C \cdot T$$

The spectral data matrix can also be considered as the multiplication of basis spectral matrix $\boldsymbol{B}$ and functional change matrix $\boldsymbol{T}$.

$$A = B \cdot T$$

Therefore, as for the reconstructed spectral data matrix A_r,

$$A_r = B \cdot T = U_r \cdot S_r \cdot V_r^T = U_r \cdot S_r \cdot C \cdot T$$

Thus, $$B = U_r \cdot S_r \cdot C$$

In our temperature-dependent experiment, we assume that the pNIPMAm nanoparticle follows the two-stage phase transtion described by a sigmodal function. ***A*** represents the swelled OMA (below LCST) and ***B*** represents the collapsed OMA (above LCST). $[A]_0$ represents the overall OMA concentration, where $[A]_0 = [A] + [B]$.

$$[A(T)] = [A]_0 \frac{exp^{-K(T - T_0)}}{1 + exp^{-K(T - T_0)}}$$

$$[B(T)] = [A]_0 \frac{1}{1 + exp^{-K(T - T_0)}}$$

where T is the temperature variable and K is the temperature-dependent equilibrium constant.

According to the above model, each vector $\boldsymbol{v_i(T)}$ of matrix $\boldsymbol{V_r^T}$ can be fit to the sigmodal function:

$$v_i(T) = c_{i1} + \frac{c_{i2}}{1 + exp^{-K(T - T_0)}}$$

Thus the 2 × 2 matrix C is determined as follow:

$$C = \begin{vmatrix} c_{11} & c_{12} \\ c_{21} & c_{22} \end{vmatrix}$$

Then we can determine basis spectral matrix ***B*** by matrix multiplication:

$$B = \sum_{i=0}^{1} b_i(\lambda) = U_r \cdot S_r \cdot C$$

As for the total absorbance of temperature-dependent spectra during the melting or cooling:

$$A_r = \varepsilon_A[A(T)] + \varepsilon_B[B(T)]$$

$$A_r = \varepsilon_A[A]_0 \frac{exp^{-K(T - T_0)}}{1 + exp^{-K(T - T_0)}} + \varepsilon_B[A]_0 \frac{1}{1 + exp^{-K(T - T_0)}}$$

$$= [A]_0 \left(\varepsilon_A + \frac{\varepsilon_B - \varepsilon_A}{1 + exp^{-K(T - T_0)}} \right)$$

where ε is the extinction coefficient profile of the measured sample.

Therefore, the absorption spectra for the swelled OMA (below LCST) and collapsed OMA (above LCST) are given below:

$$\varepsilon_A[A]_0 = b_0(\lambda)$$

$$\varepsilon_B[A]_0 = b_0(\lambda) + b_1(\lambda)$$

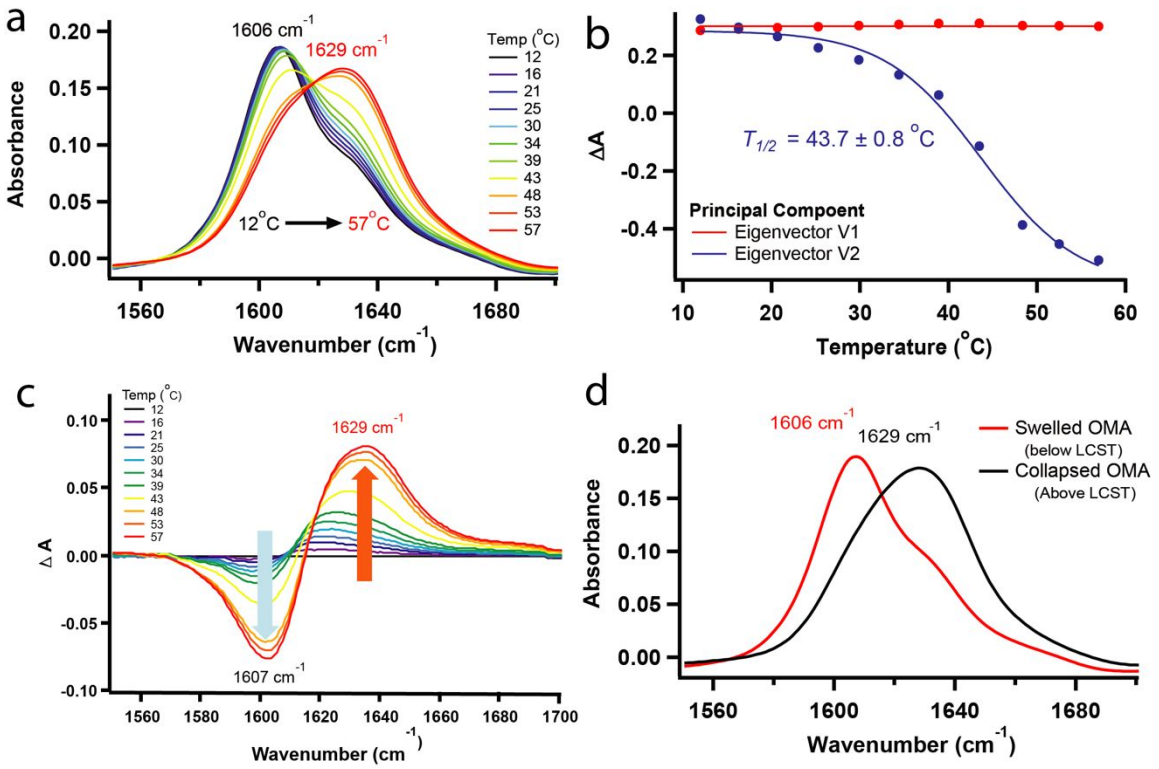

Figure S1. Temperature-dependent steady-state FTIR spectra of OMA. a) Temperature-dependent FTIR spectra of OMA during the cooling process between 12 ~ 57 °C; b) Temperature-dependent OMA swelling curve obtained from PCA of FTIR spectra; c) FTIR difference spectra of OMA during the heating process between 12 ~ 57 °C; d) Reconstructed FTIR spectra of swelled OMA and collapsed OMA obtained from PCA.

Time Course of Local T-jump Transient Infrared Absorption and Transient Near-Infrared (785 nm) Absorption Spectra

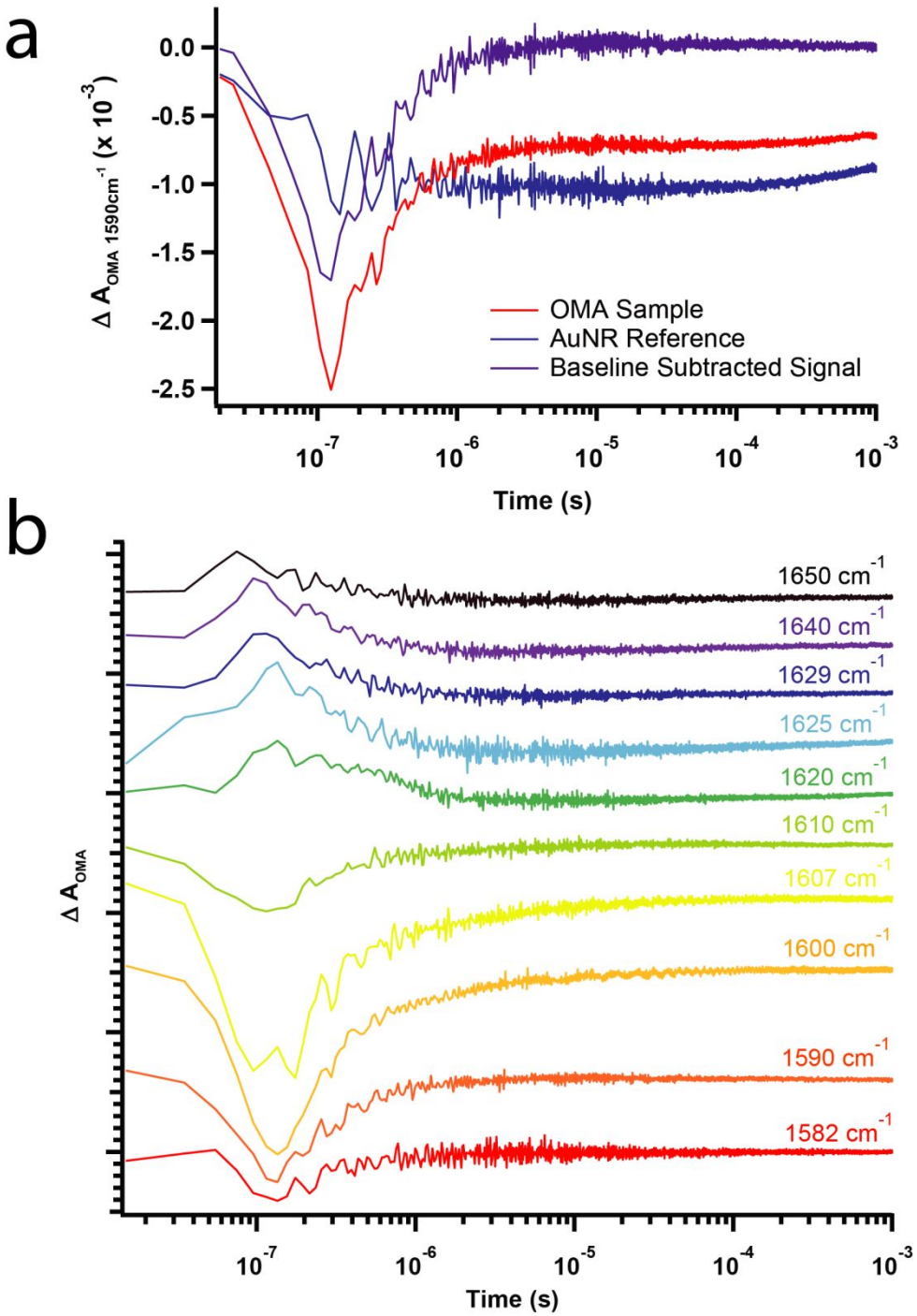

Figure S2. Local T-jump transient IR absorbance time courses at the amide I band region of OMA. The OMA concentration is ~ 0.8 nM in D_2O solvent. Each time course signal was the average of 50 measurements. a) Local T-jump transient IR absorbance of OMA sample, AuNR reference and baseline and reference subtracted signal at 1590 cm^{-1}; b) Local T-jump transient IR absorbance time course between 1582 ~ 1650 cm^{-1}.

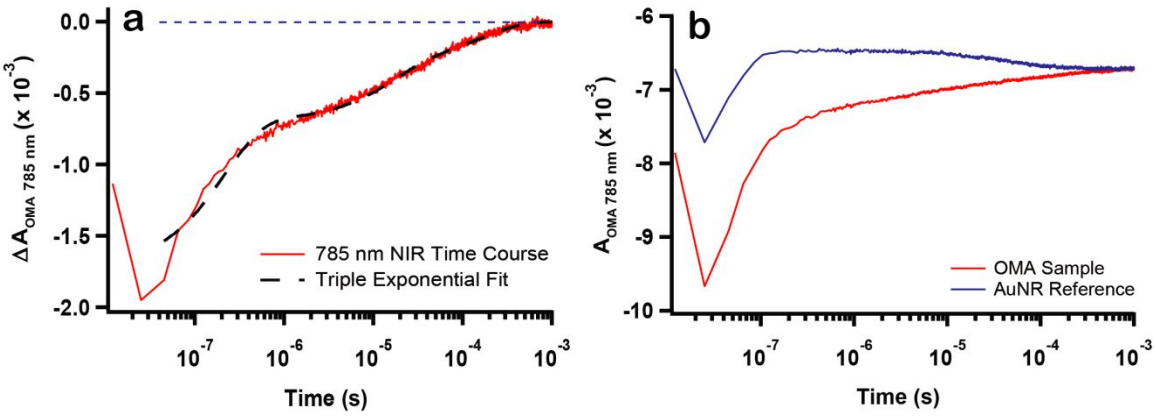

Figure S3. Transient NIR absorbance measurement of OMA at 785 nm. The OMA concentration is ~ 0.8 nM in D_2O solvent. Each time course signal was the average of 50 measurements. a) Transient NIR signal of OMA at 785 nm after subtracting AuNR reference and corresponding triple exponential fit; b) Transient NIR absorption of OMA sample and AuNR reference.

Global Heating T-Jump Time-resolved IR Spectroscopy

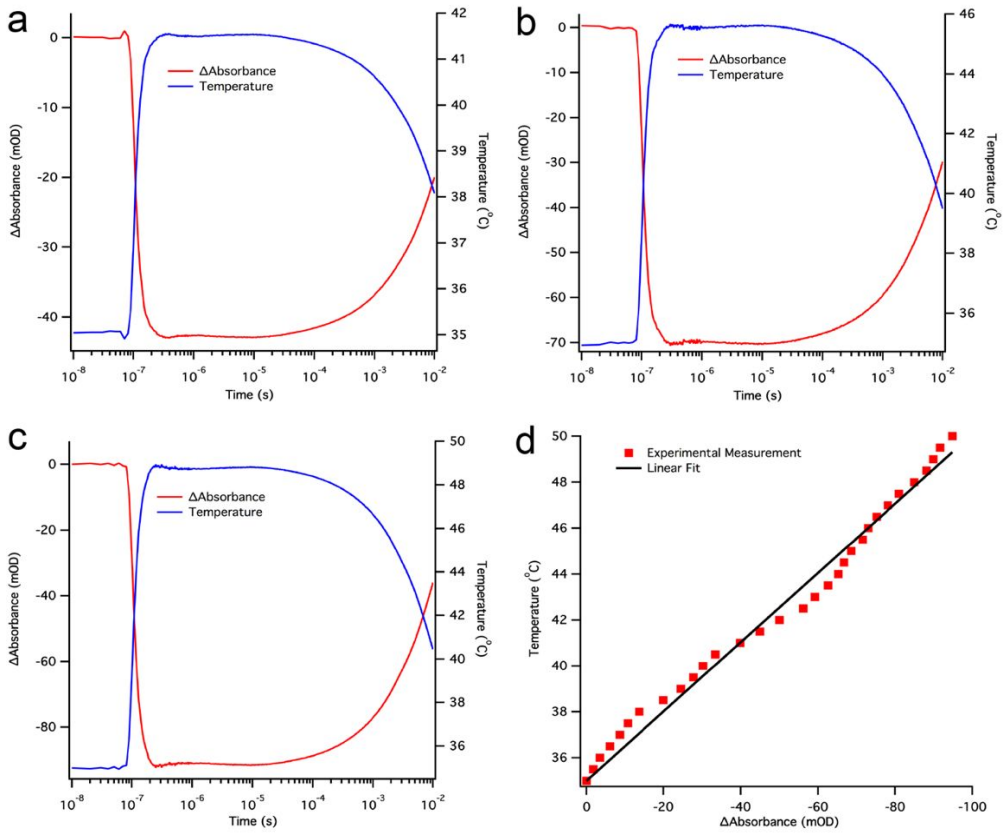

Figure S4. Time courses of global T-jump D_2O reference and temperature calibration curve.

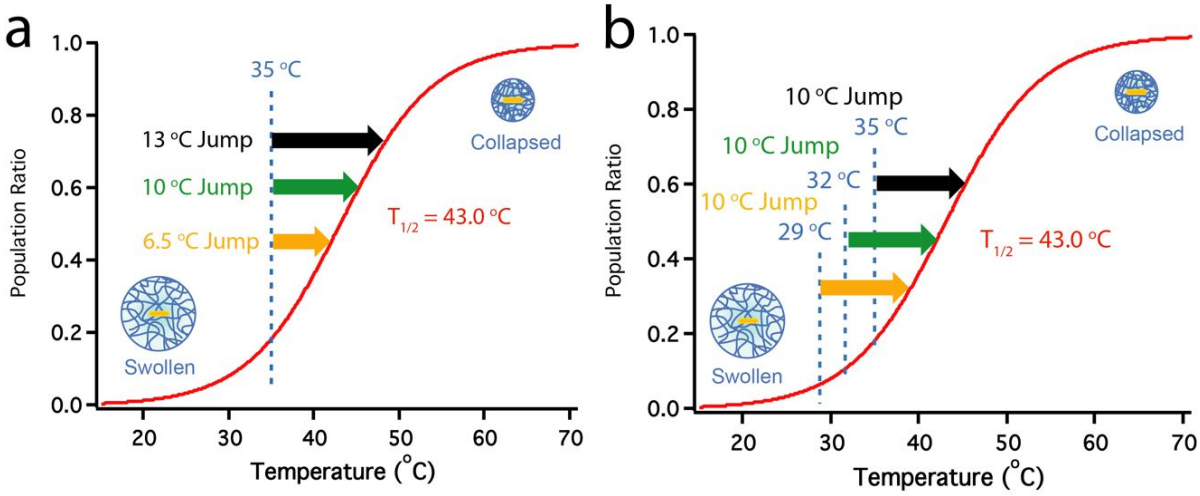

Figure S5. Schematic illustration of two groups of global T-jump IR experiments. a) Global T-Jump experiments start at 35 °C with three different temperature jumps: 6.5, 10 and 13 °C (Scheme 1); b) Global T-jump experiments start with three different starting temperatures 29, 32 and 35 *°C with the same 10 °C temperature-jump (Scheme 2).*

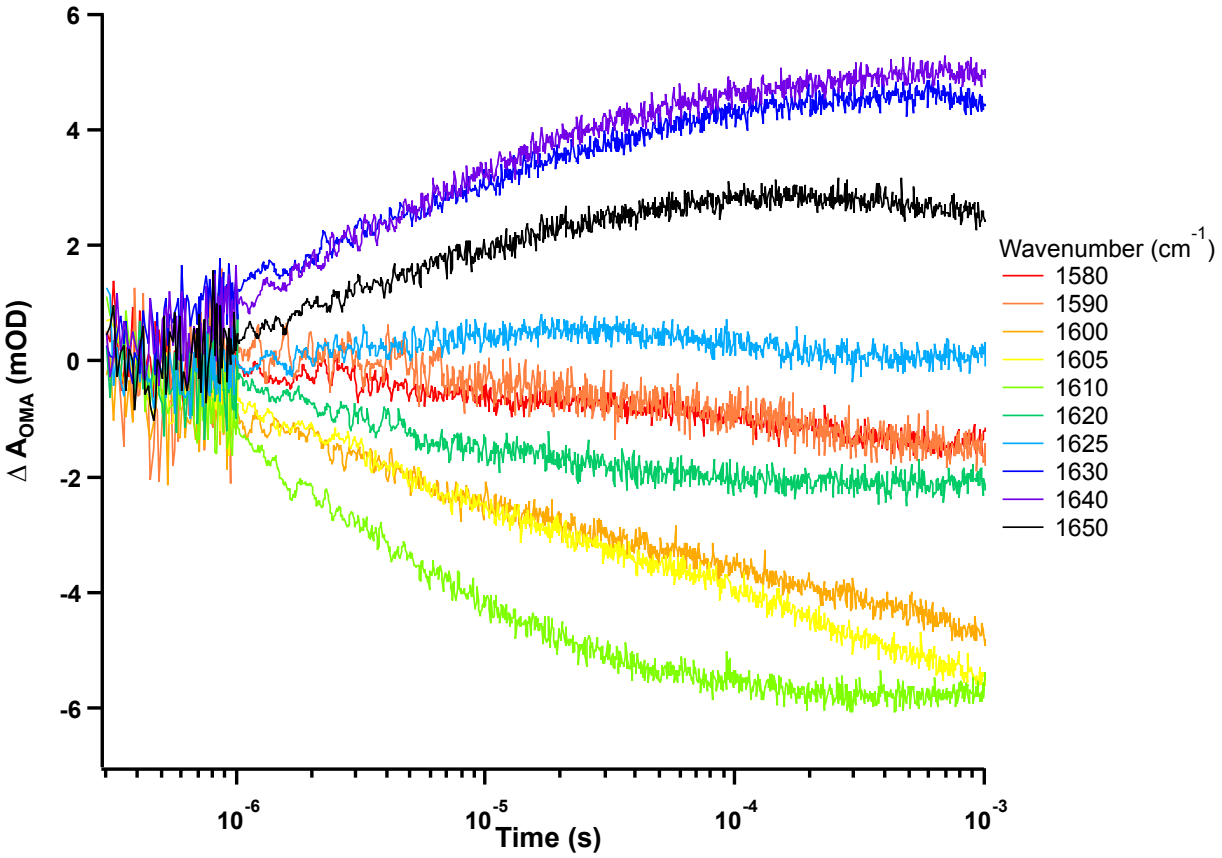

Figure S6. Time courses of global T-jump IR experiment starting at 35 °C with a 10 °C temperature jump.

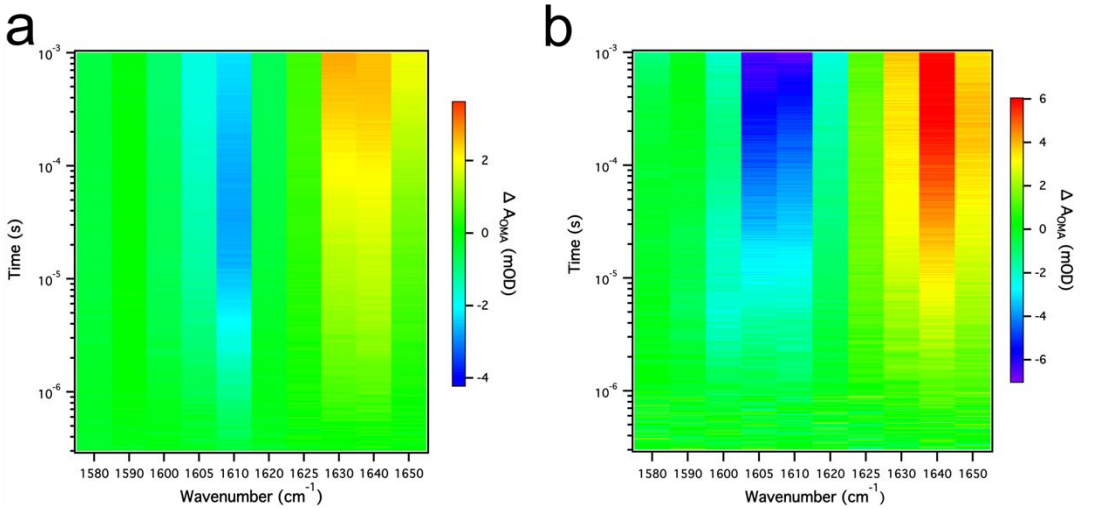

Figure S7. Global T-Jump IR spectral image of OMA. a) The spectral image of OMA measured by time-resolved global T-jump IR starts at 35 °C with a 6.5 °C temperature jump; b) The spectral image of OMA measured by time-resolved global T-jump IR starts at 35 °C with a 13 °C temperature jump.

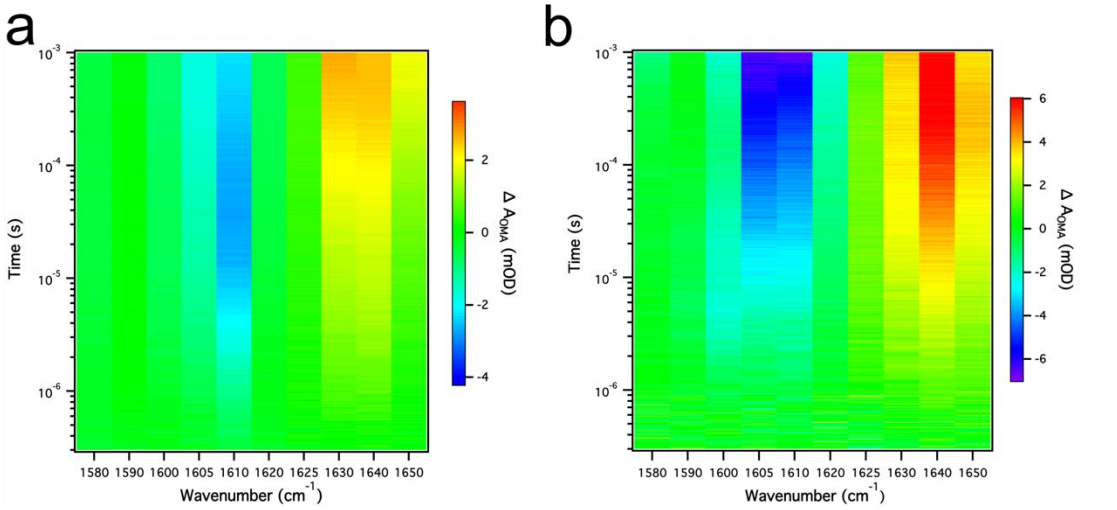

Figure S8. Global T-Jump IR spectral image of OMA. a) The spectral image of OMA measured by time-resolved global T-jump IR starts at 29 °C with a 10 °C temperature jump; b) The spectral image of OMA measured by time-resolved global T-jump IR starts at 32 °C with a 10 °C temperature jump.

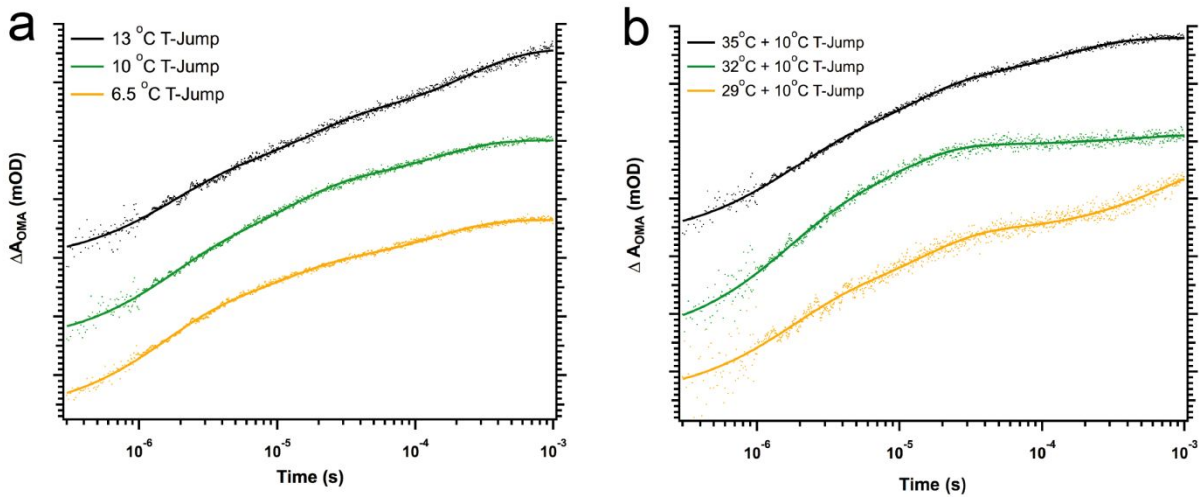

Figure S9. The time courses of global T-jump experiments. a) Three global T-jump experiments in Figure 5-scheme S1; b) Three global T-jump experiments in Figure 5-scheme S2.

The Triple-exponential function used for fitting the IR time-course is as follow:

$$y = c_0 + c_1 exp\left(-\frac{t}{\tau_1}\right) + c_2 exp\left(-\frac{t}{\tau_2}\right) + c_3 exp\left(-\frac{t}{\tau_3}\right)$$

and $$A_1 = \frac{c_1}{c_1 + c_2 + c_3} \times 100\%, \quad A_2 = \frac{c_2}{c_1 + c_2 + c_3} \times 100\%, \quad A_3 = \frac{c_3}{c_1 + c_2 + c_3} \times 100\%$$

where c_0 is the offset, and c_1, c_2, c_3 are the pre-exponential terms, A_1, A_2, A_3 are the percentage of the corresponding pre-exponential terms and τ_1, τ_2, τ_3 are the relaxation time constants.

Table S2. Triple-exponential fits of global T-jump IR deswelling kinetics of OMA in scheme S1

Start @35 °C		6.5 °C Jump		10 °C Jump		13 °C Jump	
A_1	τ_1	47.9%	1.31 ± 0.03 μs	40.7%	1.42 ± 0.05 μs	36.4%	1.50 ± 0.06 μs
A_2	τ_2	28.2%	9.45 ± 0.34 μs	36.7%	10.80 ± 0.37 μs	30.0%	14.35 ± 0.62 μs
A_3	τ_3	23.9%	139 ± 3 μs	22.6%	142 ± 5 μs	33.6%	237 ± 8 μs

Table S3. Triple-exponential fits of global T-jump IR deswelling kinetics of OMA in scheme S2

10 °C Jump		Start @29 °C		Start @32 °C		Start @35 °C	
A_1	τ_1	36.9%	1.46 ± 0.04 μs	53.3%	1.35 ± 0.06 μs	40.7%	1.42 ± 0.05 μs
A_2	τ_2	32.3%	13.1 ± 0.7 μs	41.3%	8.63 ± 0.39 μs	36.7%	10.80 ± 0.37 μs
A_3	τ_3	30.8%	754 ± 41 μs	5.4%	423 ± 149 μs	22.6%	142 ± 5 μs

COMSOL Multiphysics Simulation of Time-Dependent Heat Transfer in OMA Triggered by a Laser Pulse

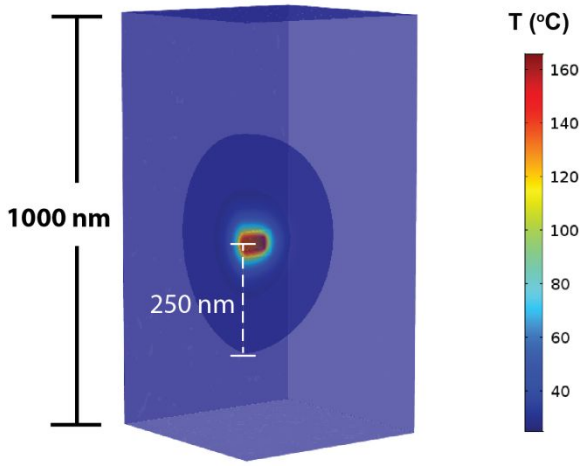

Figure S10. Three-dimensional model of OMA constructed by COMSOL Multiphysics.

The laser power absorbed by each AuNP was calculated using the following equation:

$$p_{AuNR} = \frac{p_{Laser} \times (1-\zeta)^2 \times \left(1 - 10^{-\epsilon_{AuNR} lc}\right)}{c\sigma l N_A}$$

P_{AuNR}, the laser power absorbed by AuNR in each OMA.
Assuming that the AuNR photo-thermal conversion efficiency is 100%, thus all photon energy is converted to thermal energy. Thus, P_{AuNR} is equivalent to the heating power of AuNP. Therefore, we use P_{AuNR} as the power of heating source to calculate the heat dissipation and temperature gradient in the surrounding environment in the simulations.

P_{Laser}, the laser power during the 10 ns pulse laser stimulation.
The average power of 532 nm Nd:YLF pump laser measured by the power meter at the sample is 8.2 mW. The Nd:YLF Q-switched laser is operating at 10 Hz and each with a 10 ns pulse duration. Therefore, P_{Laser} = 8.2 mW × 0.1 s/ 10 ns = 8.2 × 10^4 W during the 10 ns laser pulse.

ξ : Scattering coefficient of IR window, 0.04.

ε_{AuNR} : The molar absorption coefficient of AuNR.
$\varepsilon_{AuNR,\ 785nm}$ = 4.57 × 10^9 M^{-1} cm^{-1}. (Weihai Ni *et al*, ACS Nano, **2008, 2, 677-686)**
$\varepsilon_{AuNR,\ 785nm}$ is used to calculate the concentration of OMA sample.

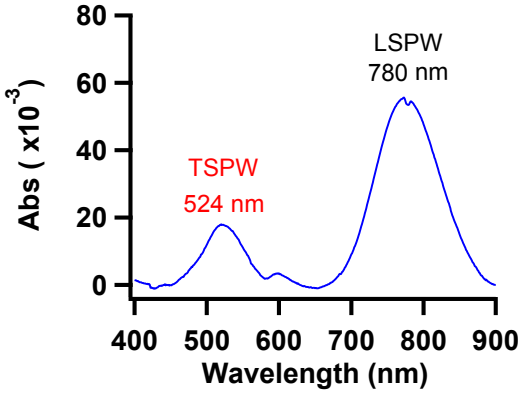

Figure S11. UV-Vis of OMA solution in IR window after baseline subtraction that removes sample scattering.

According to Beer-Lambert's law, $A_{780nm}/A_{524nm} = \varepsilon_{780nm}/\varepsilon_{524nm}$. Therefore, we can also calculate that $\boldsymbol{\varepsilon_{AuNR,\ 352nm}} = 1.46 \times 10^9\ M^{-1}\ cm^{-1}$. This is the absorbance coefficient we use to calculate the laser power absorbed by AuNR.

$\boldsymbol{l}$: The spacer distance in the IR sample window (optical pathlength), 130 μm.
$\boldsymbol{c}$: Molar concentration of OMA (AuNR) in the sample, 0.843 nM.
$\boldsymbol{N_A}$: Avogadro Number, 6.02×10^{23}.

$\boldsymbol{\sigma}$: The laser spot size of pulse laser beam. Since the diameter of the laser spot is 1 mm, thus the spot size is $7.85 \times 10^5\ \mu m^2$. The laser field intensity is $1.04 \times 10^8\ W/(cm^2 \cdot pulse)$.

Given all the parameters listed above, we can calculate that $P_{AuNR} = 5.28 * 10^{-5}$ W.

The heat transfer in the OMA can be described by the following two sets of 3-Dimensional heat transfer equations, in which variable $\boldsymbol{s}$ represents the 3D coordinate (x, y, z) in the model.
The first set of equations describe the heat transfer in AuNR and D_2O regions respectively:

$$\begin{cases} \rho_{(Au)} C_{p(Au)} \partial_t T(s,t) = \kappa_{(Au)} \nabla^2 T(s,t) + p_{AuNR}(s,t) & s \in \text{AuNR region} \\ \rho_{(w)} C_{p(w)} \partial_t T(s,t) = \kappa_{(w)} \nabla^2 T(s,t) & s \in D_2O \text{ region} \end{cases}$$

The second set of equations describe the boundary conditions that heat influx/outflux and inner surface/outer surface temperature are equal at the AuNR/D_2O interface:

$$\begin{cases} \kappa_{(Au)} \partial_r T(S^-,t) = \kappa_w \partial_r T(S^+,t) & S^- \in \text{Inner surface } of \text{ AuNR region} \\ T(S^-,t) = T(S^+,t) & S^+ \in \text{Outer surface of AuNR that in } D_2O \text{ region} \end{cases}$$

$\boldsymbol{\rho}$: density; $\boldsymbol{C_p}$: specific heat capacity; $\boldsymbol{\kappa}$: thermal conductivity.

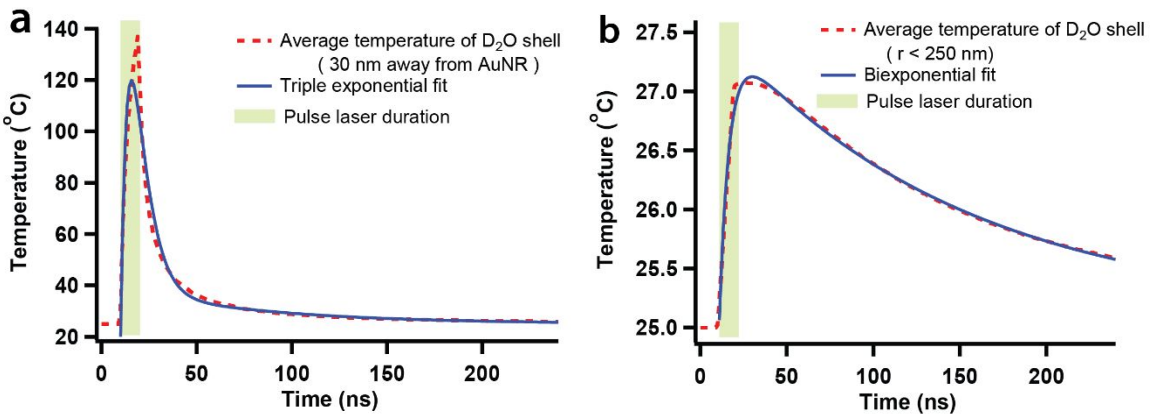

Figure S12. a) The average temperature curve of 85 × 160 nm D_2O shell during pulse laser stimulation and thermal relaxation; b) The average temperature curve of 250 nm radius D_2O shell during pulse laser stimulation and thermal relaxation.

The average temperature curves of D_2O shell that is 30 nm around AuNR was fitted into a triple exponential equation, in which the time constant for heating is $\tau_1 = 4.5$ ns and the two time constants for cooling are $\tau_2 = 6.5$ ns; $\tau_3 = 74.6$ ns. As for the average temperature curves of 250 nm radius D_2O shell, the curve was fitted to a double exponential equation, in which the time constant for heating is $\tau_1 = 5.7$ ns and the time constant for cooling is 140 ns.

Transmission Electron Microscopy Images of Gold Nanorods

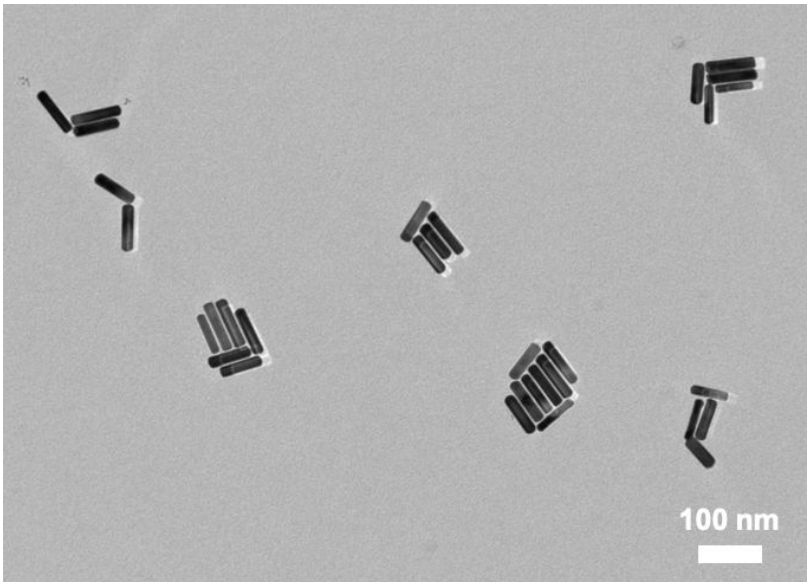

Figure S13. TEM image of gold nanorods (AuNR) with 15k magnification.